RESEARCH PAPER

Numerical simulation of metal transfer in argon gas-shielded GMAW

Yosuke Ogino · Yoshinori Hirata

Abstract The gas metal arc welding (GMAW) process combines aspects of arc plasma, droplet transfer, and weld pool phenomena. In the GMAW process, an electrode wire is melted by heat from an arc plasma, and molten metal at the wire tip is deformed by various driving forces such as electromagnetic force, surface tension, and arc pressure. Subsequently, the molten droplet detaches from the tip of the wire and is transferred to the base metal. The arc plasma shape changes together with the metal transfer behavior, so the interaction between the arc plasma and the metal droplet changes from moment to moment. In this paper, we describe a unified arc model for GMAW, including metal transfer. In the model, we do not account for heat transfer in the metal, but the wire melting rate is determined by the arc current. The developed model can show transition from globular transfer at low currents to spray transfer at higher currents. It was found that electromagnetic force is the most important factor at high currents, but surface tension is more important than electromagnetic force at low currents in determining the transfer mode.

Keywords Mathematical models · Arc physics · Metal transfer · MIG welding

1 Introduction

Gas metal arc welding (GMAW) is an indispensable industrial technology, as it is a highly productive process. It uses consumable wire electrodes and involves metal transfer phenomena. In this metal transfer, a molten metal droplet detaches from a wire tip and transfers to the base metal. Characteristics of the metal transfer such as droplet size and frequency of transfer are closely related to the stability and quality of the overall process. Therefore, appropriate control of the metal transfer process is highly desirable. However, there are many different transfer modes [1], and the process is not yet fully understood due to its complexity, so it is difficult to control the metal transfer completely. Free-flight transfer, for example, can be divided into globular transfer and spray transfer. Globular transfer occurs at low currents. In this mode, a large droplet forms at the wire tip and falls to the base metal by gravity. On the other hand, spray transfer occurs at relatively high currents. Many small droplets are sprayed onto the base metal in this mode. Spray transfer is desirable in industrial fields because of its high stability and low spatter generation.

In order to understand the metal transfer phenomena, considerable research has been performed. For example, the size of the droplet and the frequency of transfer have been observed by high-speed camera [2–4]. Especially, the globular-to-spray transition has often been discussed. Lesnewich investigated the influence of the arc current, wire diameter, and wire extension on the transfer mode and reported that the transition current became low with a small wire diameter and a small wire extension [5]. Most of the reports indicate that the transfer mode transition occurs suddenly in a narrow current range. On the other hand, there are also reports that the transition does not occur [6], that it occurs gradually [7], and that large and small droplets can coexist at the same current [8], depending on the shielding gas.

Moreover, many investigations based on numerical simulations have also been carried out since about 1960. The early phase models can be divided into two types. The first type is based on the static force balance theory [9–11], and the second is based on the pinch instability theory [12, 13]. In models

Y. Ogino (✉) · Y. Hirata
Graduate School of Engineering, Osaka University, Osaka, Japan
e-mail: ogino@mapse.eng.osaka-u.ac.jp

Fig. 1 Schematic explanation of the calculation procedure used in this model
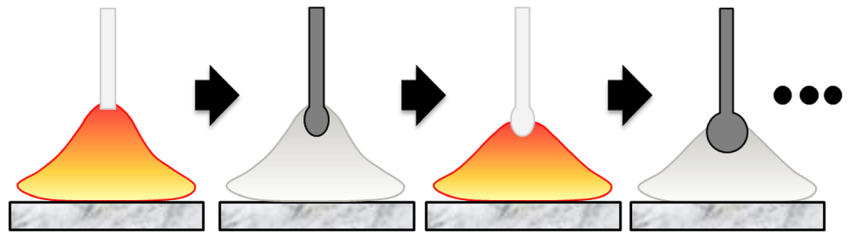
using static force balance theory, axial forces are focused and the models can calculate accurately in the globular region. The models based on pinch instability theory focus on radial forces and can calculate accurately in the spray region. Nemchinsky constructed a model including both axial and radial electromagnetic forces by assuming the current path in the droplet, and this model was accurate over a wide range of currents [14].

Recently, many dynamic models using CFD have been reported [15–17]. Wang et al. constructed a model that can describe the transition current using an assumed current density distribution on the surface of the droplet [18]. Kadota and Hirata reported the influence of material properties such as surface tension and viscosity on the size of the droplet and the transfer mode [19]. Moreover, models including heat transfer in the metal [20] and the influence of the arc plasma [21–24] have been reported. However, in these models that consider interactions between the droplet and the arc plasma, the range of calculation parameters is limited. In order to understand and control the metal transfer phenomena, a broad range of information is required. Therefore, the numerical simulations must be carried out over a wide range of process conditions.

The objective of this research is to understand the metal transfer phenomena more deeply. Therefore, a 3D numerical model including interactions between the droplet and the arc plasma was constructed, and the influence of the driving force and arc current on the metal transfer was investigated.

2 Numerical model

A numerical model that includes interactions between the metal transfer and the arc plasma was constructed in this study.
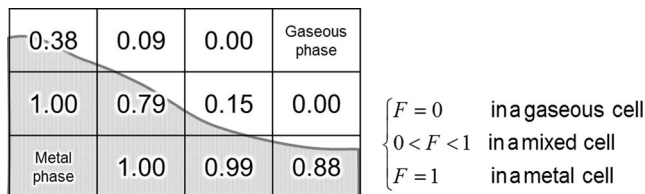
However, it is difficult to calculate these phenomena simultaneously because of difference of those material properties and velocity scales. For this reason, the arc plasma and the droplet were calculated as two separate fluids in this model. At one time step, the characteristics of the arc plasma, such as temperature, velocity, and pressure fields, are calculated first, for a fixed droplet shape. Then, the metal transfer phenomena are calculated using the arc plasma characteristics as boundary conditions. At the next time step, the arc plasma is calculated using the new droplet shape as a boundary condition. These calculations are performed repeatedly, allowing the development over time of both the droplet and arc plasma to be calculated, as shown in Fig. 1.

Metal transfer phenomena involve the deformation of a free surface, which was tracked in this model using the volume of fluid (VOF) method [25]. In the VOF method, the shape of a free surface is described by fluid occupancy using a so-called F value in each calculation cell, as shown in Fig. 2.

In this model, F was 0 when the calculation cell was filled with arc plasma (gaseous cell), and 1 when it was filled with metal (metal cell). If F was between 0 and 1, the calculation cell was considered a mixed cell, containing both arc plasma and metal. In order to improve the stability of the calculations, when the metal region was calculated, the mixed cells were calculated as mixed cells. However, for the arc plasma calculation, mixed cells whose occupancy of the arc plasma is more than 10 % were treated as gaseous cells, and the others were treated as metal cells, as shown in Fig. 3. Because of this, the calculated surface became coarse when the arc plasma was calculated.

The following method was used to calculate the arc plasma phenomena. Under the local thermodynamic equilibrium (LTE) approximation, the arc plasma can be treated as a viscous electromagnetic fluid. Therefore, the thermal and
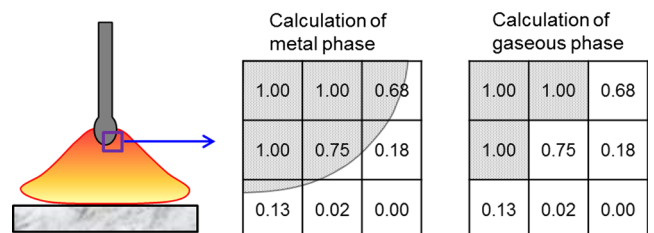

Fig. 2 Schematic diagram of the VOF method

$$\begin{cases} F = 0 & \text{in a gaseous cell} \\ 0 < F < 1 & \text{in a mixed cell} \\ F = 1 & \text{in a metal cell} \end{cases}$$

Fig. 3 Schematic explanation of the treatment of the droplet surface

Table 1 Physical properties of mild steel

Density [kg/m^3]	7200
Viscosity [Pa s]	6×10^{-3}
Surface tension [N/m]	1.2
Electrical conductivity [S/m]	7.7×10^5

electromagnetic fluid phenomena are governed by the following equations:

Mass conservation equation:

$$\nabla\cdot\left(\rho\,\vec{v}\right) = S, \tag{1}$$

Momentum conservation equation:

$$\frac{\partial\left(\rho\,\vec{v}\right)}{\partial t} + \nabla\cdot\left[\rho\,\vec{v}\,\vec{v}\right] = -\nabla P + \nabla\cdot\boldsymbol{\tau} + \rho\,\vec{g} + \vec{F}_{em}, \tag{2}$$

Energy conservation equation:

$$\frac{\partial(\rho H)}{\partial t} + \nabla\cdot\left(\rho\,\vec{v}H\right) = -\nabla\cdot(-\kappa\nabla T) + W - \text{Ra} + S_E, \tag{3}$$

where $\vec{v}$ is the velocity [m/s], t is the time [s], ρ is the density [kg/m^3], P is the pressure [Pa], $\boldsymbol{\tau}$ is the viscous stress tensor [Pa], $\vec{g}$ is the gravitational acceleration [m/s^2], H is the enthalpy [J/kg], κ is the thermal conductivity [W/m K], T is the temperature [K], Ra is the radiative loss [W/m^3], $\vec{F}_{em}$ is the electromagnetic force [N/m^3], W is the Joule heating [W/m^3], S is the source term of mass by metal vapor [kg/m^3 s], and S_E is the source term of energy by metal vapor [J/m^3 s].

The electromagnetic force and the Joule heating can be calculated using the following equations:
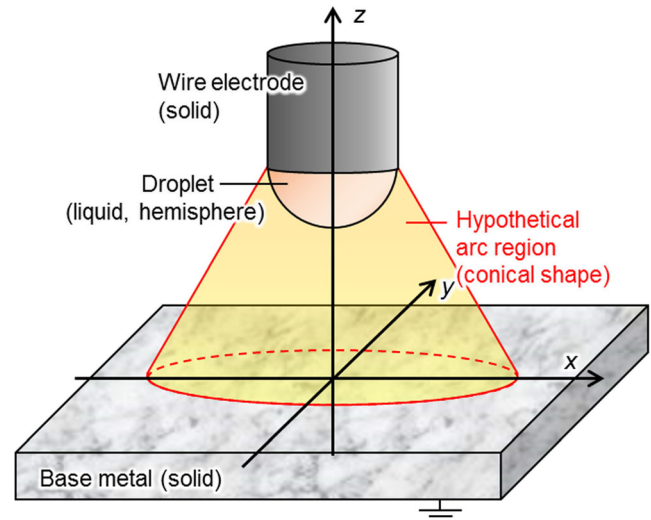
$$\vec{F}_{em} = \vec{j}\times\vec{B}, \tag{4}$$

Fig. 5 Schematic image of the hypothetical arc model with a hemispherical droplet

$$W = \frac{\left|\vec{j}\right|^2}{\sigma}, \tag{5}$$

where $\vec{j}$ is the current density [A/m^2], $\vec{B}$ is the magnetic flux density [T], and σ is the electrical conductivity [S/m]. The current density and the magnetic flux density can be calculated by the following equations:

Current conservation equation:

$$\nabla\cdot\vec{j} = 0, \tag{6}$$

Ohm's law:

$$\vec{j} = -\sigma\nabla V, \tag{7}$$

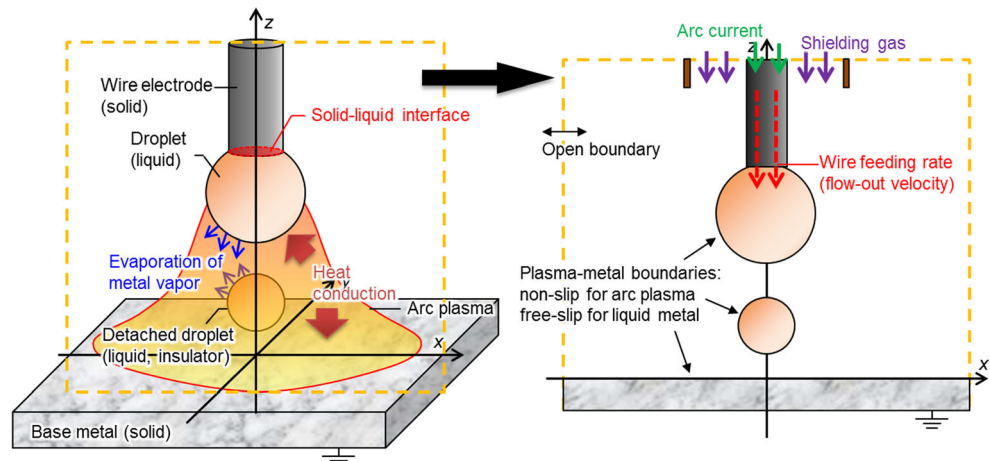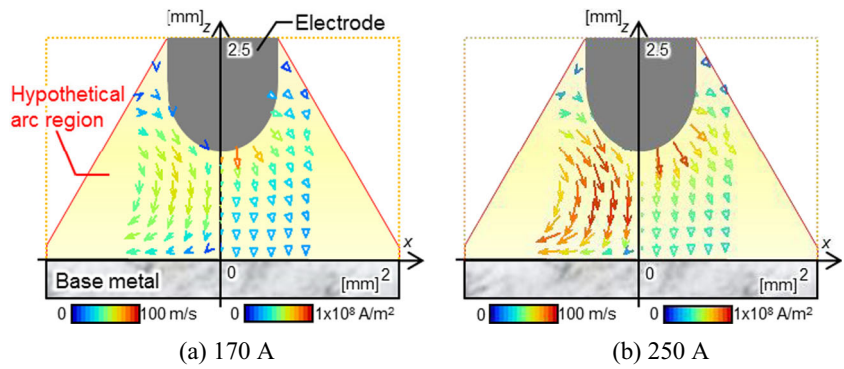**Fig. 4** Schematic image and boundary conditions of the simulation model

Fig. 6 Velocity and current density distribution in the hypothetical arc region: **a** 170 A, **b** 250 A

(a) 170 A (b) 250 A

Magnetic flux density and vector potential:

$$\vec{B} = \nabla \times \vec{A}, \tag{8}$$

$$\nabla^2 \vec{A} = -\mu_0 \vec{j}, \tag{9}$$

where V is the electric potential [V], $\vec{A}$ is the vector potential [N/A], and μ_0 is the permeability of free space [H/m].

In this model, the influence of the iron vapor is considered. Iron vapor is only generated from the tip of the electrode and the droplet, and its distribution can be described using the following equation:

$$\frac{\partial(\rho C)}{\partial t} + \nabla \cdot \left(\rho \vec{v} C \right) = \nabla \cdot (\rho D \nabla C) + S, \tag{10}$$

where C is the mass fraction of iron vapor and D is the diffusion coefficient [m²/s] [26]. The iron vapor is generated according to the following equation:

$$J = \left(\frac{p_0}{\sqrt{T_{\text{metal}}}} - \frac{p_{\text{Fe,gas}}}{\sqrt{T_{\text{gas}}}} \right) \sqrt{\frac{M}{2\pi R}}, \tag{11}$$

where J is the mass flux of iron vapor [kg/m² s], p_0 is the saturated vapor pressure of the iron vapor [Pa], $p_{\text{Fe,gas}}$ is the partial pressure of iron vapor in arc plasma [Pa], T_{metal} is the temperature of the metal [K], T_{gas} is the temperature of the arc plasma adjacent to the metal [K], M is the molecular weight of iron [kg/mol], and R is the gas constant [J/mol K]. S in Eq. (1) and S_E in Eq. (3) were calculated using the following equations:

$$S = -\nabla \cdot \vec{J}, \tag{12}$$

$$S_E = -\nabla \cdot \left(H_{\text{vap}} \vec{J} \right), \tag{13}$$

where H_{vap} is the vaporization heat of iron [J/kg], $\vec{J} = -J\hat{n}$, and $\hat{n}$ is the unit normal vector calculated from the shape of the droplet.

Fig. 7 Driving force distribution on the hemispherical droplet. **a** 170 A: *i* surface tension, *ii* electromagnetic force, *iii* arc pressure, *iv* drag force. **b** 250 A: *i* surface tension, *ii* electromagnetic force, *iii* arc pressure, *iv* drag force

(i) Surface tension (ii) Electromagnetic force (iii) Arc pressure (iv) Drag force
(a) 170 A
(i) Surface tension (ii) Electromagnetic force (iii) Arc pressure (iv) Drag force
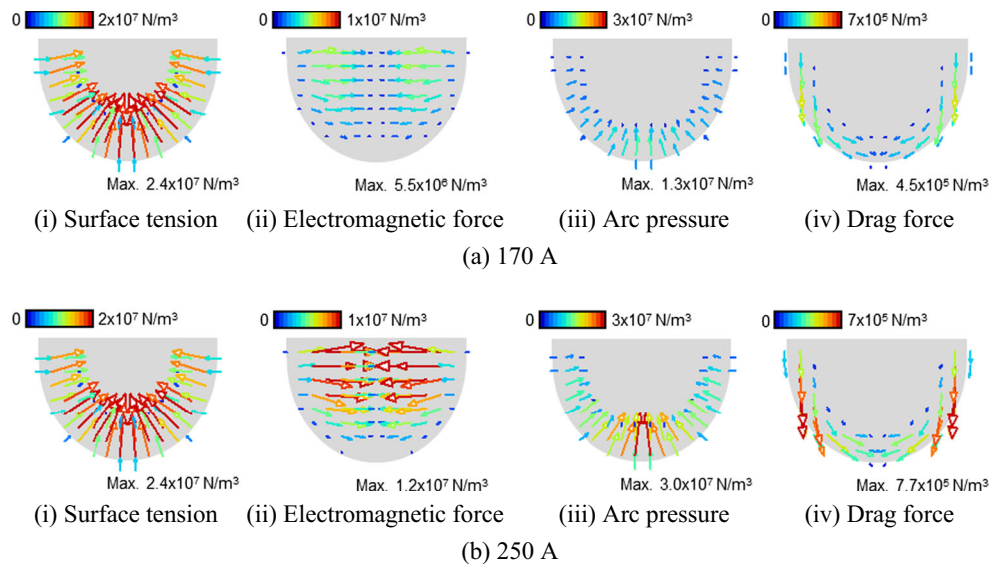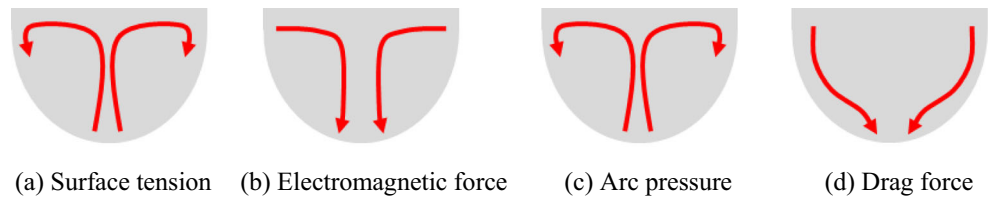(b) 250 A

Fig. 8 Schematic image of the velocity field in the droplet: **a** surface tension, **b** electromagnetic force, **c** arc pressure, **d** drag force

(a) Surface tension (b) Electromagnetic force (c) Arc pressure (d) Drag force

In this study, the shielding gas was argon. However, the material properties of the plasma gas are changed remarkably by the influence of the iron vapor. In this model, the material properties of the plasma gas were taken from a paper by Murphy [27]. The radiation loss of argon was calculated using the method reported by Cram [28], and that of the iron vapor was calculated using Menart's method [29]. The flow of heat from the arc plasma to the droplet and the base metal by conduction is described by the following equation:

$$\overrightarrow{q}_S = -\kappa_S \nabla T, \tag{14}$$

where $\overrightarrow{q}_S$ is the heat flux between the arc plasma and the metal [W/m²] and κ_S is the thermal conductivity of the boundary between the arc plasma and the metal [W/m K]. κ_S was calculated from the average temperature T_S [K], obtained using the following equation:

$$T_S = \frac{T_{gas} + T_{metal}}{2}. \tag{15}$$

Next, the calculation method of the droplet is explained. In this model, heat transfer in the metal region is neglected. The liquid metal flows out from the interface between solid and liquid according to the wire feed rate, and the temperature of the liquid metal is constant. The temperature of the solid region of the wire and the base metal was set to 300 K. The

position of the interface between solid and liquid was determined from a balance between the wire melting rate and the wire feed rate. In this model, the wire melting rate was always equal to the wire feed rate, and the interface was fixed at a certain position. The governing equations of the metal region were as follows:

Mass conservation equation:

$$\nabla \cdot \overrightarrow{v} = -\frac{S}{\rho}, \tag{16}$$

Momentum conservation equation:

$$\frac{\partial \overrightarrow{v}}{\partial t} + \nabla \cdot \left[\overrightarrow{v}\,\overrightarrow{v} \right] = -\frac{1}{\rho}\nabla P + \frac{1}{\rho}\nabla \cdot \boldsymbol{\tau} + \overrightarrow{g} + \frac{1}{\rho}\overrightarrow{F}_{ex}, \tag{17}$$

where $\overrightarrow{F}_{ex}$ is the external force vector [N/m³]. This is a summation of the electromagnetic force, the surface tension, the arc pressure, and the drag force by plasma stream. According to the velocity field in the metal region, the free surface deformation is calculated using the following equation:

$$\frac{\partial F}{\partial t} + \left(\overrightarrow{v} \cdot \nabla \right) F = 0. \tag{18}$$

The surface tension force was calculated using the CSF model [30], in which the capillary pressure of surface tension

Fig. 9 Influence of surface tension on the droplet shape. **a** 170 A: *i* initial condition, *ii* all driving forces, *iii* surface tension only. **b** 250 A: *i* initial condition, *ii* all driving forces, *iii* surface tension only
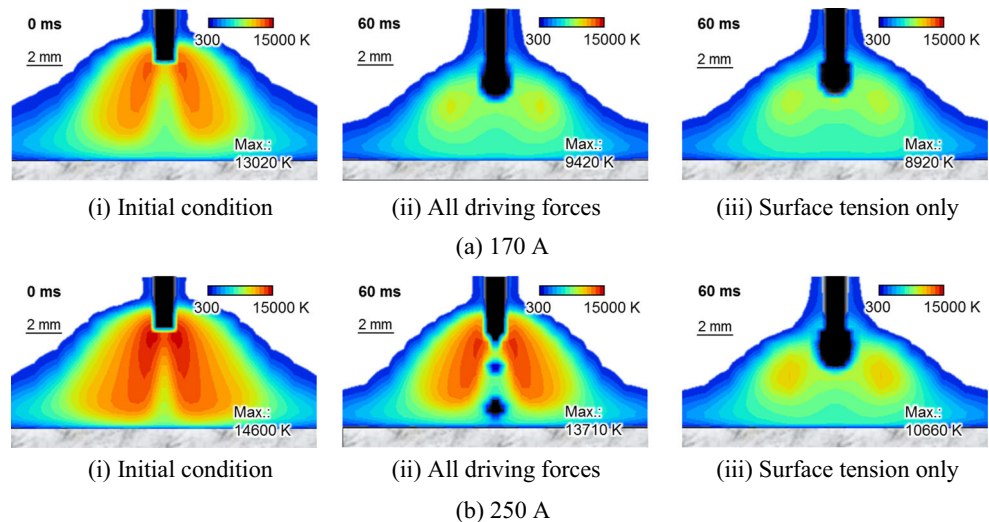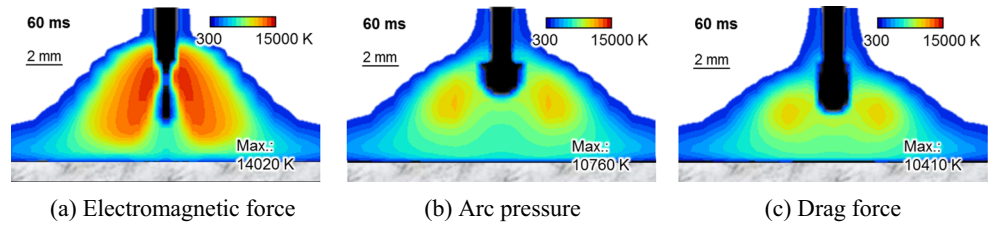
(i) Initial condition (ii) All driving forces (iii) Surface tension only

(a) 170 A

(i) Initial condition (ii) All driving forces (iii) Surface tension only

(b) 250 A

Fig. 10 Influence of driving force on the droplet shape (arc current 250 A): **a** electromagnetic force, **b** arc pressure, **c** drag force

(a) Electromagnetic force   (b) Arc pressure   (c) Drag force

acting on the liquid phase is expressed as a volume force in the surface region. This can be calculated as follows:

$$\overrightarrow{F}_{ST} = \gamma \kappa_{curv} \overrightarrow{n}, \tag{19}$$

where $\overrightarrow{F}_{ST}$ is the equivalent volume force vector of the capillary pressure of the surface tension [N/m³], γ is the surface tension [N/m], κ_{curv} is the curvature [1/m], and $\overrightarrow{n}$ is the normal vector [1/m]. These are the governing equations of the metal transfer phenomena. The wire electrode was mild steel, and its diameter was 1.2 mm. The constant values shown in Table 1 were used as the electrode's material properties [31].

Figure 4 shows a schematic image of the model used, along with the boundary conditions employed. The metal transfer and the arc plasma were calculated in the same 3D domain. The current density and shielding gas were applied at the top boundary. The solid region of the wire and the base metal was not allowed to flow or deform. The droplet that detached from the wire tip was treated as an insulator, and the base metal and torch were stationary. The wire feed rate was equal to the wire melting rate, which was calculated using the following equation:

$$v_{m} = \alpha I + \beta E_{x} I^{2}, \tag{20}$$

where v_{m} is the wire melting rate [m/s], α and β are constants depending on the radius and other properties of the wire, I is the arc current [A], and E_{x} is the wire extension [m]. The constants α and β were obtained from experimental results,

and their values were $\alpha = 3.11 \times 10^{-4}$ m/A s and $\beta = 4.63 \times 10^{-5}$ 1/A² s [32].

3 Driving forces in the metal transfer phenomena

3.1 Driving forces acting on the pendant drop

In this section, the influence of the driving forces acting on the droplet on the metal transfer is investigated. Here, a hemispherical droplet was positioned at the wire tip, and a hypothetical arc region was located between the droplet and the base metal. The hypothetical arc was conical in shape. Figure 5 shows a schematic image of this calculation, in which the material properties in the hypothetical arc region were those of pure argon at 10,000 K, and the properties in the region outside the hypothetical arc were those of pure argon at 1000 K. The shape of the droplet and the hypothetical arc did not change during the calculation. In this calculation, the minimum spatial mesh size was 0.1 mm×0.1 mm×0.1 mm, and the time discretization was 5×10^{-5} s.

The calculated velocity and current density distribution under these conditions are shown in Fig. 6. The arc currents were 170 and 250 A. In the figures, the left side shows the velocity field, and the right-hand side shows the current density distribution. When the arc current was high, the velocity and the current density increased. Therefore, for high currents, the electromagnetic force and plasma drag force increased.

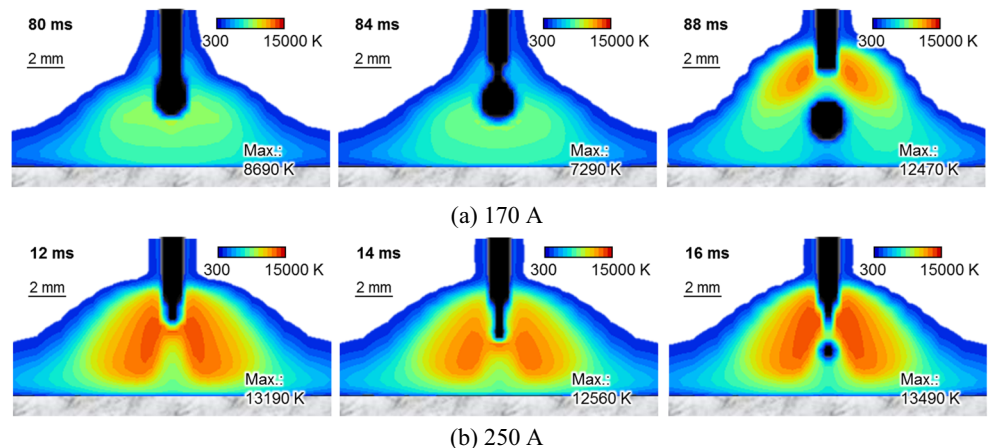**Fig. 11** Calculated temperature fields in the arc plasma and droplet shapes: **a** 170 A, **b** 250 A

(a) 170 A

(b) 250 A

Fig. 12 Calculated electrical conductivity and current density distributions in the arc plasma: **a** 170 A, **b** 250 A
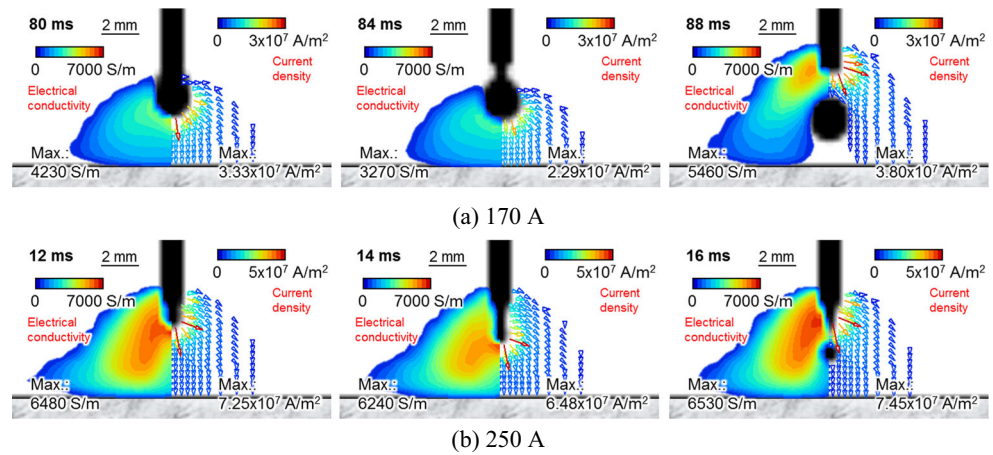

(a) 170 A

(b) 250 A

Figure 7 shows the driving forces acting on the pendant droplet. These figures show (a) the surface tension, (b) the electromagnetic force, (c) the arc pressure, and (d) the plasma drag force. The values shown have been converted to body forces. The surface tension was independent of the arc current because it was determined by the shape of the droplet. However, the other driving forces had higher values at higher currents.

Therefore, when the arc current was low, it was presumed that the material properties of the wire became relatively important in determining the transfer mode. The driving forces act as follows. The surface tension acts to raise the droplet. The electromagnetic force pinches the top of the droplet. The arc pressure acts to raise the droplet, just like the surface tension. The plasma drag force drags the droplet downward but is weaker than the other forces. Therefore, the surface tension and arc pressure resist the transition to spray transfer, while the electromagnetic force and the plasma drag force promote the transition to spray transfer. Figure 8 shows a schematic image of the velocity fields induced by each driving force.

However, the calculated driving force changes with changes in the properties of the droplet and the hypothetical arc. In an actual arc plasma, the current path is very complicated due to the temperature distribution and the influence of the metal vapor. Moreover, the droplet and arc plasma shapes change continuously. Therefore, the metal transfer occurs in the presence of changes in both the temperature distribution in the arc plasma and the driving forces acting on the droplet.

3.2 Influence of the driving forces on the metal transfer phenomena

Next, the influence of the driving forces was investigated in the case of continuous changes in both the arc plasma and the droplet using the model constructed in this study. In these calculations, the minimum spatial mesh size was 0.3 mm × 0.3 mm × 0.3 mm, and the time discretization was 5×10^{-7} s in the arc region and 1×10^{-4} s in the metal region. In this model, we considered four driving forces. The surface tension was determined by the material properties and droplet shape, while the others were determined by the properties of the arc

Fig. 13 Calculated velocity and iron vapor concentration distributions in the arc plasma: **a** 170 A, **b** 250 A

(a) 170 A

(b) 250 A
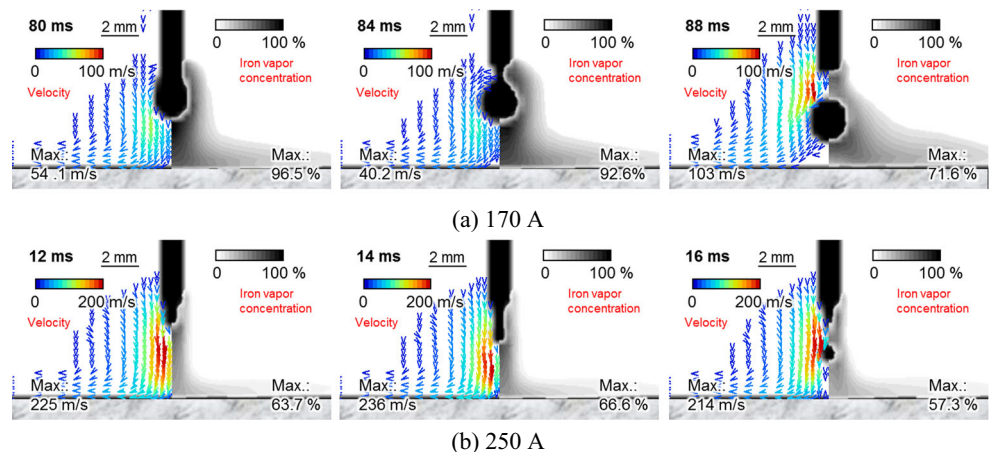
plasma. Moreover, the surface tension is required to maintain an appropriate droplet shape. Here, the influence of the surface tension is investigated first.

Figure 9 shows the calculated temperature distributions in the arc plasma and the droplet shape when all of the driving forces act on the droplet, and also when only the surface tension acts on the droplet. The black area shows the droplet and the solid wire. Figure 9a(i), b(i) shows the initial conditions of the calculation, and the others show calculated results 60 ms after the beginning of the calculation. In this calculation, the wire temperature was 2500 K, and the distance from the interface between the liquid and solid wire to the base metal surface was 5 mm. At an arc current of 170 A, the droplet shapes were very similar. However, at 250 A, the shapes were significantly different. These results indicate that surface tension is the dominant factor in the metal transfer when the arc current is low and that the properties of the arc plasma have a strong influence at high currents.

Figure 10 shows the calculated results in which the electromagnetic force, the arc pressure, and the plasma drag force acted separately on the droplet. The arc current was 250 A. In these calculations, the surface tension acted on the droplet. These results are very similar to those shown in Fig. 9b(ii) when only the electromagnetic force acted on the droplet. Therefore, for high arc currents, the electromagnetic force is the dominant factor in determining the transfer mode. These results are in good agreement with the results reported by Lowke, which were calculated using a simple model to analyze the transition current from globular to spray transfer [33].

4 Time variation of the arc plasma during metal transfer

The properties of the arc plasma, such as the temperature field, change with the growth and detachment of a droplet. Figure 11 shows the time variation of the temperature distribution of the arc plasma and the droplet shape for arc currents of 170 and 250 A. In this calculation, the wire temperature was 2500 K, and the distance from the interface between the liquid and solid wire to the base metal surface was 5 mm. When the arc current was 170 A, the droplet grew larger than the electrode wire. This is globular transfer. At 250 A, the droplet was small, and the transfer mode was spray transfer. This is because when the arc current is high, the electromagnetic force also becomes high, causing a strong pinching effect to act on the droplet. The droplet becomes elongated downward at first. Then, the droplet constricts and subsequently detaches from the wire. The temperature field of the arc plasma changes along with the droplet behavior. When a droplet is growing at the wire tip, the temperature of the arc plasma decreases.

When the droplet detaches from the wire tip, a high-temperature region forms near the wire tip.

Figure 12 shows the electrical conductivity and current density distributions. When a droplet is growing at the wire tip, the electrical conductivity and current density at the bottom of the droplet are high. When the droplet detaches from the wire tip, the current density concentrates at the wire tip. Joule heating is dependent upon the current density, and the temperature distribution changes as shown in Fig. 11.

Figure 13 shows the velocity and iron vapor distribution in the arc plasma. As shown in the figure, the velocity is low for a large droplet. This is easily observable at 170 A. When the droplet detaches from the wire tip, the plasma velocity at the wire tip increases considerably. This is because the electromagnetic force distribution changes, as do the current density and Joule heating. The iron vapor distribution is concentrated at the center of the arc plasma, and this leads to lower temperatures at the center of the arc plasma. In this calculation, when the arc current was low, the iron vapor was more concentrated. In this case, the mass flux of iron vapor was the same because the wire temperature was the same. When the arc current was low, the surface area of the droplet was large and the velocity of the arc plasma was low. Therefore, the iron vapor could easily remain within the arc plasma.

5 Influence of the arc current on the transfer frequency

Figure 14 shows the influence of the arc current on the transfer frequency of the droplet. In this figure, the experimental results reported by Hirata [34] are also shown for reference. As shown in the figure, the frequency of droplet transfer becomes high when the arc current is high. In this calculation, the transition from globular to spray transfer does not occur suddenly, but gradually. At an arc current of 190 A, there was a mixture of large and small droplets.
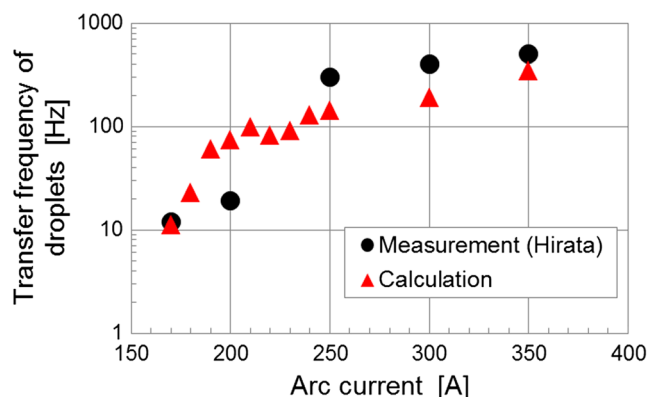

Fig. 14 Influence of the arc current on the droplet transfer frequency

6 Conclusion

In this study, in order to clarify the metal transfer phenomena in gas metal arc welding, a numerical model including interactions between the droplets and the arc plasma was constructed. The results obtained are summarized as follows:

1. When the arc current is low, surface tension is the dominant factor determining the metal transfer mode. At high currents, electromagnetic force becomes the dominant factor.
2. The temperature and velocity distribution of the arc plasma change with changes in the current density distribution.
3. When the arc current is high, the transfer frequency of the droplet becomes high and spray transfer becomes the dominant transfer mode.
4. In this calculation, the transition from globular to spray is gradual, not sudden.
5. The numerical model constructed in this study can be used over a wide range of arc currents.

References

1. Ruckdeschel WEW (1976) Classification of metal transfer. IIW Doc. XII-636-76
2. Ludwig HC (1957) Metal transfer characteristics in gas-shielded arc welding. Weld J 36:23s–26s
3. Needham JC, Cooksey CJ, Milner DR (1960) Metal transfer in inert-gas shielded-arc welding. Br Weld J 7:101–114
4. Liu S, Siewert TA (1989) Metal transfer in gas metal arc welding: droplet rate. Weld J 68:52s–58s
5. Lesnewich A (1958) Control of melting rate and metal transfer in gas-shielded metal-arc welding part II—control of metal transfer. Weld J 37:418s–425s
6. Rhee S, Kannatey-Asibu E Jr (1992) Observation of metal transfer during gas metal arc welding. Weld J 71:381s–386s
7. Kim Y-S, Eagar TW (1993) Analysis of metal transfer in gas metal arc welding. Weld J 72:269s–278s
8. Jones LA, Eagar TW, Lang JH (1998) Images of a steel electrode in Ar-2%O2 shielding during constant current gas metal arc welding. Weld J 77:135s–141s
9. Greene WJ (1960) An analysis of transfer in gas-shielded welding arc. Trans AIEE Part 2 7:194–203
10. Amson JC (1965) Lorentz force in the molten tip of an arc electrode. Br J Appl Phys 16:1169–1179
11. Waszink JH, Graat LHJ (1983) Experimental investigation of forces acting on a drop of weld metal. Weld J 62:108s–116s
12. Allum CJ (1985) Metal transfer in arc welding as a varicose instability: I. Varicose instabilities in a current-carrying liquid cylinder with surface tension. J Phys D Appl Phys 18:1431–1446
13. Allum CJ (1985) Metal transfer in arc welding as a varicose instability: I. Development of model for arc welding. J Phys D Appl Phys 18:1447–1468
14. Nemchinsky VA (1994) Size and shape of the liquid droplet at the molten tip of an arc electrode. J Phys D Appl Phys 27:1433–1442
15. Simpson SW, Zhu P (1995) Formation of molten droplet at a consumable anode in an electric welding arc. J Phys D Appl Phys 28:1594–1600
16. Choi SK, Yoo CD, Kim Y-S (1998) Dynamic simulation of metal transfer in GMAW, part 1: globular and spray transfer modes. Weld J 77:38s–44s
17. Choi SK, Yoo CD, Kim Y-S (1998) The dynamic analysis of metal transfer in pulsed current gas metal arc welding. J Phys D Appl Phys 31:207–215
18. Wang G, Huang PG, Zhang YM (2003) Numerical analysis of metal transfer in gas metal arc welding. Metall Mater Trans B 34B:345–353
19. Kadota K, Hirata Y (2011) Numerical model of metal transfer using an electrically conductive liquid. Weld World 55:50–55
20. Wang F, Hou WK, Hu SJ, Kannatey-Asibu E, Schultz WW, Wang PC (2003) Modelling and analysis of metal transfer in gas metal arc welding. J Phys D Appl Phys 36:1143–1152
21. Haidar J, Lowke JJ (1996) Predictions of metal droplet formation in arc welding. J Phys D Appl Phys 29:2951–2960
22. Hu J, Tsai HL (2007) Heat and mass transfer in gas metal arc welding. Part II: the metal. Int J Heat Mass Transf 50:808–820
23. Xu G, Hu J, Tsai HL (2009) Three-dimensional modeling of arc plasma and metal transfer in gas metal arc welding. Int J Heat Mass Transf 52:1709–1724
24. Hertel M, Spille-Kohoff A, Fuessel U, Schnick M (2013) Numerical simulation of droplet detachment in pulsed gas-metal arc welding including the influence of metal vapour. J Phys D Appl Phys 46:224003
25. Hirt CW, Nichols BD (1981) Volume of fluid (VOF) method for the dynamics of free boundaries. J Comput Phys 39:201–225
26. Wilke CR (1950) A viscosity equation for gas mixtures. J Chem Phys 18(4):517–519
27. Murphy AB (2010) The effect of metal vapour in arc welding. J Phys D Appl Phys 43:434001
28. Cram LE (1985) Statistical evaluation of radiative power losses from thermal plasmas due to spectral lines. J Phys D Appl Phys 18:401–411
29. Menart J, Malik S (2002) Net emission coefficients for argon-iron thermal plasmas. J Phys D Appl Phys 35:867–874
30. Brackbill JU, Kothe DB, Zamach C (1992) A continuum method for modeling surface tension. J Comput Phys 100:335–354
31. Rao ZH, Hu J, Liao SM, Tsai HL (2010) Modeling of the transport phenomena in GMAW using argon–helium mixtures. Part I—the arc. Int J Heat Mass Transf 53:5707–5721
32. Hirata Y (1994) Physics of welding—melting rate and temperature distribution of electrode wire. J Jpn Weld Soc 63(7):484–488 (in Japanese)
33. Lowke JJ (2009) Physical basis for the transition from globular to spray modes in gas metal arc welding. J Phys D Appl Phys 42:135204
34. Hirata Y (2003) Pulsed arc welding. Weld Int 17:98–115